Creep and Hysteresis Compensation in Pressure-Sensitive Mats for Improving Center-of-Pressure Measurements

Javier Martínez-Cesteros, Carlos Medrano-Sánchez, *Senior Member, IEEE*, Julián Castellanos-Ramos, José A. Sánchez-Durán, and Inmaculada Plaza-García, *Senior Member, IEEE*

***Abstract*—Large-area tactile sensors are used to image the pressure exerted by human body parts. More specifically, they can be used to measure plantar pressure on human stability tests. The center-of-pressure (CoP) trajectory is the primary outcome of such tests. Previous research has shown that the parameters obtained from the trajectory correlate with those obtained from a reference instrument, that is, a force platform (FP). However, there are still noticeable differences. In this work, a low-cost prototype of a pressure-sensitive mat (PSM) has been built and compared with an FP in stability tests. The sensitive material is Velostat, which is readily available. Such a mat could make objective stability tests more accessible. A model of two nonlinear effects, hysteresis and creep, has been considered to compensate for them. Given that it was rather difficult to characterize the large mat with a pneumatic device, a small-sized sensor array was first characterized in a controlled environment. Then the model was extended to the large mat using a suitable scaling factor. The experimental results show that compensating for the nonlinear effects led to a decrease in the differences between the two instruments, the FP and the mat, with an average improvement of 26% in the distance between the trajectories.**

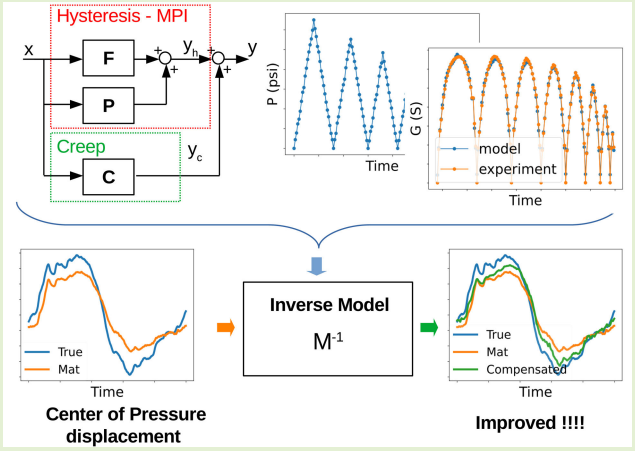

***Index Terms*— Center of pressure (CoP), creep, force platform (FP), hysteresis, resistive sensor array, stability test, tactile sensor.**

I. Introduction

PRESSURE sensor arrays have been used in the field of robotics, ergonomics, or sports among many others. In this article we focus on large area sensors, pressure-sensitive mats (PSMs), suitable for imaging the pressure of body parts on seats or on the floor [1], [2].

One of the parameters that can be obtained from a pressure distribution is the center of pressure (CoP). Its displacement is a typical measurement in balance tests [3], [4], [5]. The instrument that can be considered the gold standard for measuring CoP is the force platform (FP). However, they are usually expensive and cumbersome. Thus, several alternatives have been proposed. PSMs are one of them, the outstanding benefits of which are low weight, flexibility, ease of transportation, and cost in some cases. Several studies [6], [7], [8], [9], [10] have compared both systems by extracting some parameters of the CoP trajectory that have shown moderate to strong correlation. The differences are not surprising given that the principle of operation is completely different. In PSMs, there are several sensing units in which capacitance or resistance change when a force is applied. The response of each unit is far from an ideal straight line and several phenomena such as nonrepeatability, creep, hysteresis, or nonlinearity appear very often [11], [12], [13], [14], [15]. If the units are placed in an array, crosstalk can appear too [16]. Besides, it is

Manuscript received 13 September 2023; accepted 6 October 2023. Date of publication 19 October 2023; date of current version 30 November 2023. This work was supported in part by the MCIN/AEI/10.13039/501100011033, in part by the "ERDF A way of making Europe" under Grant PID2021-125091OB-I00, and in part by the Departamento de Ciencia, Universidad y Sociedad del Conocimiento del Gobierno de Aragón under Grant T49_20R. The work of Javier Martínez-Cesteros was supported by the Spanish "Ministerio de Ciencia, Innovación y Universidades" under Grant FPU-18/04282. The associate editor coordinating the review of this article and approving it for publication was Prof. Bernhard Jakoby. *(Corresponding author: Javier Martínez-Cesteros.)*

This work involved human subjects or animals in its research. Approval of all ethical and experimental procedures and protocols was granted by the Comité de Ética de la Investigación de la Comunidad Autónoma de Aragón (CEICA) under Application No. 22/2019, and performed in line with the Validación de una malla sensorizada para la medida de los movimientos del centro de presión.

Please see the Acknowledgment section of this paper for the author affiliations.

This article has supplementary downloadable material available at https://doi.org/10.1109/JSEN.2023.3324363, provided by the authors.

Digital Object Identifier 10.1109/JSEN.2023.3324363

well-known that each cell in an array has a different response even if the manufacturing process, material, and electrode shape are the same for all of them. Thus, an equilibration step is often recommended [17]. In [10] it was shown that removing crosstalk, improving resolution, and modeling of sensor time response could improve agreement between the instruments. In [6], the agreement between both instruments was improved by considering a filter in the frequency domain that relates their CoP displacements. The filter was found numerically.

One aspect that remains to be studied is the influence of hysteresis and creep in the CoP derived from a PSM. Hysteresis and creep compensation is very common in piezoelectric actuators [18], [19]. The compensation requires a model of the hysteresis and dynamic behavior of the actuator. Once the model is known, the simplest control strategy is a feedforward operation in which the inverse model is placed in cascade with the piezoactuated stage [19], [20]. In this way, the influence of creep and hysteresis is minimized. For tactile sensors, hysteresis can also be compensated as in [21]: a generalized Prandtl–Ishlinskii model was used to model the sensor output. In this way, the compensated pressure reduced its error from 7.20% to 1.51% for an input range of 206 kPa. A large error reduction was also found by using a Preisach hysteresis model for a silicon piezoresistive sensor [22]. In [23], a new model of hysteresis was implemented in order to better predict the output of a tactile sensor on a printed circuit board (PCB). It was shown that fitting an individual model for each taxel in a 16×16 array improved pressure images dramatically, reducing not only the hysteresis nonlinearities but also the mismatching between different taxels. In [24], a modified Prandtl–Ishlinskii (MPI) model was used to compensate for the hysteresis of a piezoresistive sensor and reduce the error in estimating the rotation angle of a wrist. Arndt [25] considered a simple model to correct the creep in a plantar pressure measurement system. The tests were performed with two subjects, who walked for three hours. The boots included commercial insoles with capacitive sensors. Creep was determined by fitting a second-order polynomial on the total force output to calculate the percentage of increase in sensor output. Then this percentage was used to correct the output of specific sensors. It was found that the corrected force underneath the metatarsal heads II–V was in agreement with previous fatigue studies. In [26], creep was corrected for a foam rubber optical pressure system. The strain was modeled as the addition of an instantaneous response and an exponential term. This model was found to be better than power law time-dependent functions. A different approach to compensation was presented in [27]. In this study, the force applied to a flexible tactile sensor based on carbon black–filled elastomers was recovered using a new probabilistic nonparametric sensor model based on Gaussian processes. In comparison with other Gaussian process filtering, the proposed approach reduced the error by 33%.

The goal of the current study is to compensate for nonlinear effects of piezoresistive sensors to improve CoP measurements. The compensation is performed for a large area mat composed of an array of 16×16 cells. Each cell contains an interdigital electrode and a Velostat as sensitive material. This material has become popular for low-cost devices [12], [28]. The focus is on applications to human balance tests. However, a small-sized array was also constructed to find the hysteresis and creep models because the large area mat could not fit into the pneumatic device used for characterizing the sensor response.

The novelty of this article relies on several aspects. First of all, the hysteresis and creep of a pressure sensor based on Velostat has been modeled. Although there have been several studies that have measured properties of Velostat-based tactile sensors such as sensitivity, hysteresis, response time, creep, or repeatability (see [11], [14], [28], [29], [30] or [31] and references therein), they just characterize these phenomena with simple parameters extracted from the sensor response. On the other hand, the current work uses a theory with a strong formal background to develop the model and opens the possibility of compensation by inverting it. Second, the compensation is applied to improve CoP measurements. Previous studies that compared FP and PSM did not try to carry out any improvement [7], [8], [9] or did not consider hysteresis at all [6], [10]. In any case, they do not consider the CoP itself but some quantities derived from it. Thirdly, no previous studies on tactile sensors have considered the joint compensation of creep and hysteresis. In this regard, only hysteresis was considered in [21], [22], [23], [24], and [27], while only creep was considered in [25] and [26]. Fourthly, in the current paper the model found for the small-sized array is extended to the large area mat. Given that it is not possible to characterize the mat itself, a scaling factor is introduced to adapt the model found in the small-sized array. This heuristic factor ensures that the total pressure detected by the mat is coherent with the weight of the person on it. On the other hand, in previous studies [21], [22], [23], [24], [25], [26], [27] the models were found in the same experiments for which compensation was then carried out. Finally, it is worth pointing out that our study deals with a low-cost PSM with poor accuracy, many sources of error, and mismatching between cells. Despite this, it is shown that the CoP measurement can be improved with the proposed compensation. Therefore, this study promotes the availability of reliable and affordable instruments for stability measurements, which are performed everyday in primary health care centers.

The remainder of this article is organized as follows. Section II presents the models of asymmetric hysteresis and creep together with the figures of merit to evaluate performance and the rationale behind the use of a scaling factor. Section III presents the experimental set-up, which includes the pneumatic device, a commercial FP and a prototype of PSM. The FP is the reference instrument. Moreover, the tests performed by several volunteers are also described. Section IV presents and discusses the results of the experiments: on one hand, the results found on the pneumatic device to find the model parameters; on the other hand, the results found on the stability tests to check the improvement due to the correction of nonlinear effects. Finally, Section V outlines the main conclusions and guides for future research.

II. Theoretical Background

A. Hysteresis

In this article, we have adopted an MPI model to compensate for the hysteresis behavior [32]. It belongs to the group of phenomenological models based on operators [19]. It has several advantages: it can be inverted analytically and the equations are described in [32]; it relies on a few parameters, which is very suitable to find them in a fitting process; it can model asymmetric hysteresis, which appear often in previous studies.

The hysteresis behavior is based on the one-side play (OSP) operator, which is a modification of the play operator for positive signals. Given an input $x(t)$ for t in $[0, t_M]$ and a set of times $0 < t_1 < t_2 < \cdots < t_M$ so that $x(t)$ is monotone in each subinterval $[t_i, t_{i+1}]$, the output of the OSP operator, $y_r(t)$, with threshold r is as follows:

$$\begin{aligned} y_r(0) &= F_r[x](0) = f_r(x(0), 0) \\ y_r(t) &= F_r[x](t) = f_r(x(t), y_r(t_i)) \end{aligned} \tag{1}$$

for $t_i < t \leq t_{i+1}$, with

$$f_r(x, y_r) = \max(x - r, \min(x, y_r)). \tag{2}$$

The output of the system is obtained from a weighted sum of OSP operators. Besides, a third-order polynomial is added to model asymmetric hysteresis

$$y_h(t) = a_1\, x(t) + a_2\, x^2(t) + a_3 x^3(t) + \sum_{i=1}^{N} b_i\, F_{r_i}[x](t). \tag{3}$$

In this article, we have selected $N = 6$ OSP operators with equally distributed thresholds as $r_i = (i-1)/N$ considering a normalized input. Moreover the weights are given as a typical decreasing exponential function with two parameters, ρ and τ

$$b_i = \rho\, e^{(-\tau\, r_i)}. \tag{4}$$

To define the inverse of the MPI model [32], the output is divided as a sum of two parts

$$y_h(t) = P[x](t) + F[x](t) \tag{5}$$

where $P[x](t) = a_2\, x^2(t) + a_3 x^3(t)$ and $F[x](t) = a_1\, x(t) + \sum_{i=1}^{N} b_i\, F_{r_i}[x](t)$. Thus $F[x](t)$ represents the hysteresis and the linear term.

The inverse F^{-1} is again an MPI model [32]

$$F^{-1}[u](t) = \hat{a}_1\, u(t) + \sum_{j=1}^{N} \hat{b}_j\, F_{\hat{r}_j}[u](t) \tag{6}$$

where

$$\begin{aligned} \hat{a}_1 &= \frac{1}{a_1} \\ \hat{b}_j &= -\frac{b_j}{\left(a_1 + \sum_{i=1}^{j-1} b_i\right)\left(a_1 + \sum_{i=1}^{j} b_i\right)} \\ \hat{r}_j &= a_1\, r_j + \sum_{i=1}^{j-1} b_i (r_j - r_i). \end{aligned} \tag{7}$$

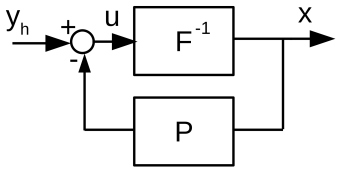

Fig. 1. Signal flowchart of the inverse hysteresis operation.

In order to get the complete inverse model, the flowchart of Fig. 1 can be applied [32]. In other words, to obtain $x(t)$ from $y_h(t)$, we apply the following equations:

$$\begin{aligned} u(t) &= y_h(t) - P[x](t) = y_h(t) - (a_2\, x^2(t) + a_3\, x^3(t)) \\ x(t) &= F^{-1}[u](t). \end{aligned} \tag{8}$$

B. Creep

A single creep operator can be modeled as a first-order linear time invariant model [18], [19]. In the time domain, the global creep can be represented by a weighted sum of creep operators [33], [34], [35]. Each creep operator has a parameter l_i and produces an output at time $t_k = k\,T$ given by

$$y_{c,i}(t_k) = e^{-l_i\, T}\, y_{c,i}(t_{k-1}) + (1 - e^{-l_i\, T}) x(t_{k-1}) \tag{9}$$

where T is the sampling period.

The total creep output, represented as $C[x](t)$, is given by

$$y_c(t_k) = C[x](t_k) = \sum_{i=1}^{N_c} w_i\, y_{c,i}(t_k) \tag{10}$$

where w_i is the weight and N_c is the number of creep operators.

C. Joint Creep and Hysteresis Modeling

The joint model of hysteresis and creep is given in Fig. 2(a). The outputs of hysteresis and creep, (3) and (10), are added [34]. The joint inverse model is better understood graphically, Fig. 2(b), applying the same ideas as in Fig. 1 [36]. Formally, the output is again obtained as $x(t) = F^{-1}[u](t)$, with $F^{-1}[u](t)$ defined in (6). However, in this case the creep is also subtracted to get $u(t)$

$$u(t) = y(t) - P[x](t) - C[x](t) \tag{11}$$

where $P[x](t)$ is defined below (5), and $C[x](t)$ is defined in (10).

In our study, the sensor input, x, corresponds to pressure, and the sensor output, y, to its conductance. Thus, the inverse model can be used to recover the applied pressure from the measured conductance.

D. Parameter Identification

The set of all model parameters is the following: ρ, τ, (a_1, a_2, a_3), l_i, and w_i. Their identification is not a trivial task. It is an optimization problem in a high dimensional space with several constraints. If a pressure temporal series, x_t, is applied to a sensor and the conductance of the sensor is recorded

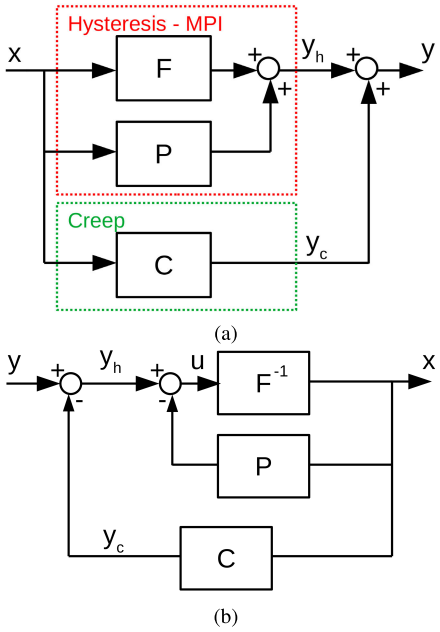

Fig. 2. (a) Signal flowchart of the joint hysteresis and creep model and (b) its inverse.

as $y_{\text{exp},t}$, then the goal is to minimize the sum of squares of the difference between the experimental output, $y_{\text{exp},t}$, and the model output, $y_{m,t}$, which in this article is also divided by the number of points in the sequence, N_t. Thus, the target function to be minimized, SSE_N, is defined as follows:

$$\text{SSE}_N = \frac{\sum_{t=1}^{N_t}(y_{\text{exp},t} - y_{m,t})^2}{N_t}. \tag{12}$$

It is typical to use some stochastic search algorithm. Thus, in this article, we have adopted a simulated-annealing algorithm [37] for searching the parameter space.

E. Extending the Model to a Large Mat

As it will be explained in Section III, it was not possible to characterize directly the PSM used in the stability test, which is a 32 × 32 cm mat. Thus, the model parameters were found for a reduced sensor array. However, this leads to the question of the suitability of the given model for a different array, even if the materials and electrode shapes are the same.

In this article, a heuristic scaling factor is proposed for the stability experiments in which a person stands on the large mat. If the model that relates conductance to pressure is called generically as $x = M(y)$, then the conductance is scaled by a factor f such that

$$\sum_{i=1}^{16}\sum_{j=1}^{16} M(f \cdot y_{i,j}) \cdot A = \text{Weight} \tag{13}$$

where $y_{i,j}$ is the conductance measured for each cell of the mat, A is the area of the cells, and Weight is the weight of the volunteer performing the experiment. The mat used in this article is a square array of 16 × 16 cells.

The stability experiments lasted 30 s so that we took the average of the above equation. The factor f was found by means of a brute force search in the interval $[0.25, 0.75]$.

F. CoP Trajectory Comparison and Model Variants

When comparing the output of the large mat and the FP, the figure of merit, Eu, is based on the comparison of the CoP trajectories given by the two instruments. We considered the distance between each pair of points of a trajectory, d_i and obtained the lock-step Euclidean distance [38], which is further divided by the number of points in the trajectory, N_{CoP}

$$Eu = \frac{\sqrt{\sum_{i=1}^{N_{\text{CoP}}} d_i^2}}{N_{\text{CoP}}}. \tag{14}$$

Several model variants are considered in Section IV to check the improvement associated with increasing model complexity: a naive approach in which conductance and pressure is supposed to be proportional, a compensation of hysteresis and creep using the model found in the pneumatic platform, and the same compensation including the scaling factor described in Section II-E.

III. Experimental Set-Up

A. Experiments for Model Identification

The experiments for identification of creep and hysteresis parameters were done with a small-sized array of ten sensors because the large mat did not fit into the pneumatic device used for characterization. The electrode had an interdigital shape manufactured on a PCB and was covered with a sheet of Velostat. This material is a carbon-impregnated polyolefin foil (surface resistivity < 31 kΩ/cm^2, volume resistivity $<$ 500 Ω-cm, thickness 0.2 mm). A simple multiplexed data acquisition system based on an Arduino Nano Every Board and a voltage divider circuit was used to read the sensor data and send them to a PC.

The small-sized array was introduced in a pneumatic device suitable for applying a series of predefined uniform pressures. The pneumatic characterization system consists of a PB100E Equilibration Device by Tekscan [39] (gauge accuracy: 1% F.S., pressure range: 0–100 psi) controlled with a proportional pressure regulator 171E2N.T.D.0009 by Pneumax [40] (linearity: $<\pm$0.3% F.S., hysteresis: $<$0.3% F.S., repeatability: $<\pm$0.3% F.S., sensitivity $< \pm$0.3% F.S., outlet pressure: 0–9 bar). This pressure regulator is connected to a personal computer to control the exerted pressure automatically using LabVIEW$^{\text{TM}}$ application. Fig. 3 shows a photo of the characterization set-up and a scheme of the system connections.

A set of hysteresis cycles was applied: changing the maximum pressure value first (descendent hysteresis cycles) and later the minimum one (ascendant hysteresis cycles). The pressure changed every 6 s (2 psi step). Before changing the pressure set point, both pressure and conductances were recorded. In the descendent hysteresis set, one cycle involves exerting pressure from 0 to 32 psi. Another cycle is done from 0 to 28 psi (4 psi lower than the last maximum value), and so on, until eight cycles are completed. In the ascendant hysteresis set, one cycle consists in applying pressure from 0 to 32 psi, then down to 4 psi (4 psi higher than the last minimum value), up again until 32 psi, and finally down to 0 psi; and so on until seven cycles are completed. Each set of cycles was repeated ten times consecutively.

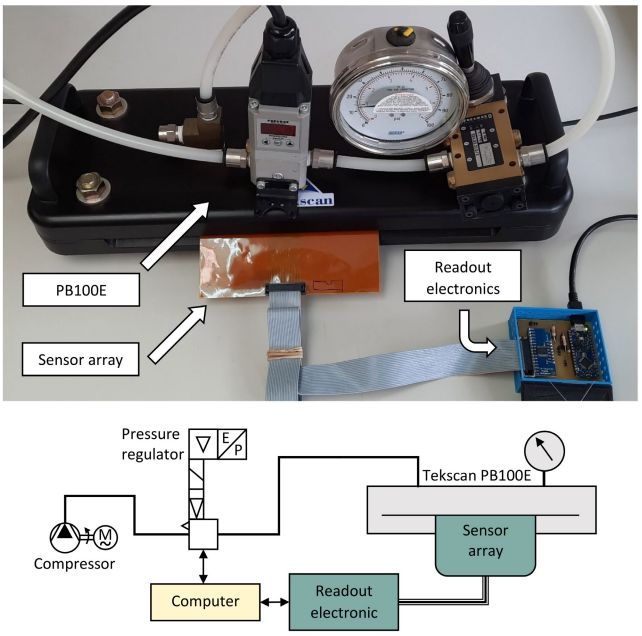

Fig. 3. Experimental set-up with the pneumatic device.

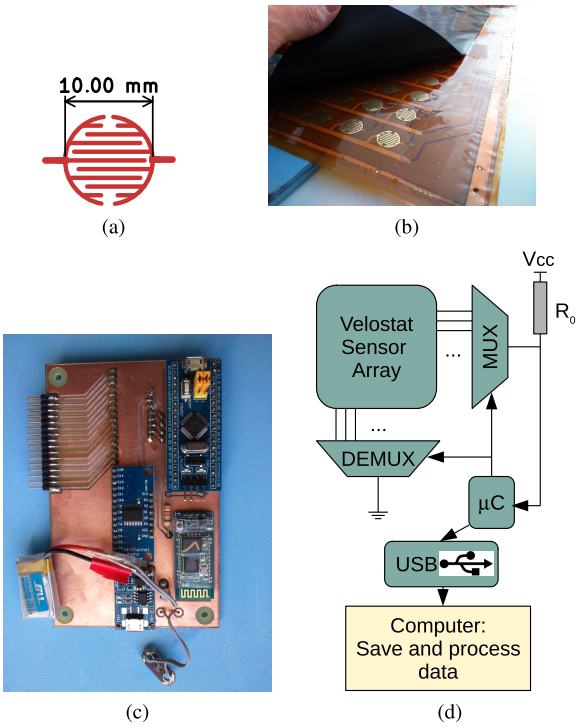

Fig. 4. Prototype of PSM. (a) Electrode shape. (b) Corner of the PSM with unfolded sheet of Velostat. (c) Picture of the data acquisition system. (d) Diagram of the data acquisition system.

In this study, the output of the ten sensors was averaged and considered as a single unit. The model identification was performed for this averaged sensor.

B. PSM Prototype and Stability Tests

The CoP was measured simultaneously by a commercial FP and the PSM prototype. The FP was a PS-2141 PASPort by PASCO [41] (weight: 4 kg, size 35 × 35 cm). It allows measuring forces between −1100 and 4400 N with a resolution of 0.1 N. The measurements were registered at 100 Hz. The PASCO software records data via USB, performs some processing, and exports the data to a file in which the CoP coordinates are stored directly.

The prototype PSM is based on a 16 × 16 grid of interdigital electrodes [Fig. 4(a)] on a flexible PCB, covering an area of 32 × 32 cm. A sheet of piezoresistive Velostat was attached to the PCB to provide pressure sensitivity. Fig. 4(b) shows a picture of the PSM. Analog multiplexers select one cell at a time, which is connected to a voltage divider circuit and to the ADC of an STM32F103C8T6 microcontroller. Data is sent to a PC via USB [Fig. 4(c) and (d)], which also powers the circuit. The whole PSM is scanned at 100 Hz. The circuit is similar to those described in [10], [42], and [43]. It also allows Bluetooth communication and battery power but these options were not used in this study. This basic circuit shows crosstalk [16] that was removed using a post-processing [44], [45]. The CoP was obtained from the pressure measurements.

The PSM was placed on top of the FP during the experiments. Then, data acquisition was started. Afterward, each volunteer was asked to step on the instruments and perform a test for at least 30 s while trying to control balance. Thus, the mat started from an unloaded condition in all the tests, allowing the inverse model to be applied from a known state. Three kinds of tests were performed[1]: 1) single-legged, left leg; 2) single-legged, right leg; and 3) starting in quiet standing and then swaying while describing circles seen from above ("rotation" test for short). In the rotation test, the CoP describes an elliptic path approximately. The CoP span is higher than in the single-legged experiments because the movements are somehow forced. In this way, instruments can be compared for different ranges. Given that the data acquisition software is different for each instrument, they were not synchronized. Therefore their CoP signals had an unavoidable delay. A semi-automatic procedure based on their cross correlation was used to align them and extract a 30-s window for further processing. Since only relative displacements are interesting in human balance studies, in both instruments coordinates were measured with respect to their average values in each axis. This allows a fair comparison between them. In this way, the exact position of the PSM on top of the FP is not relevant, although the PSM was approximately centered on the FP surface.

Four volunteers performed the tests. Each participant consented to the experimental protocol, which was approved by the regional ethics committee: Comité de Ética de la Investigación de la Comunidad Autónoma de Aragón (CEICA), on December 18, 2019, (reference: 22/2019, protocol version: 1.0, 29-11-2019).

[1]Videos showing how tests were carried out have been uploaded as supplementary material. Code and data associated with the article is publicly available at https://gitlab.com/ctmedra1/creep_hyst_comp_psm/-/releases/v202310

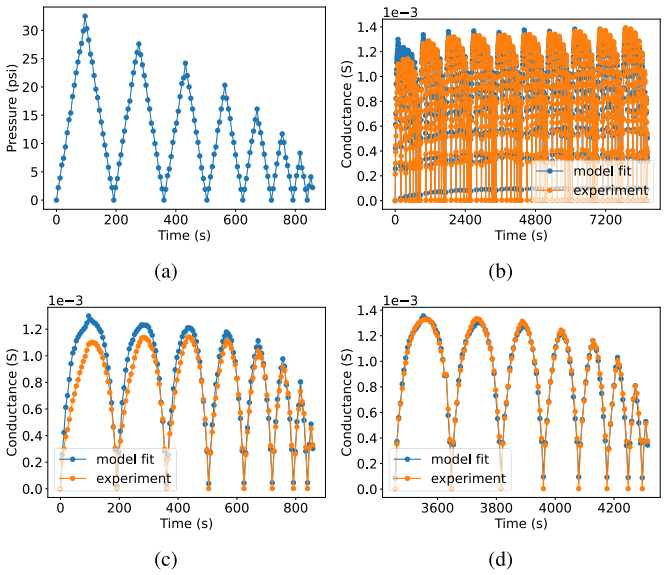

Fig. 5. Experimental results of the descendent hysteresis cycles. (a) Pressure pattern applied in one repetition. (b) General view of ten repetitions. (c) First repetition. (d) Fifth repetition.

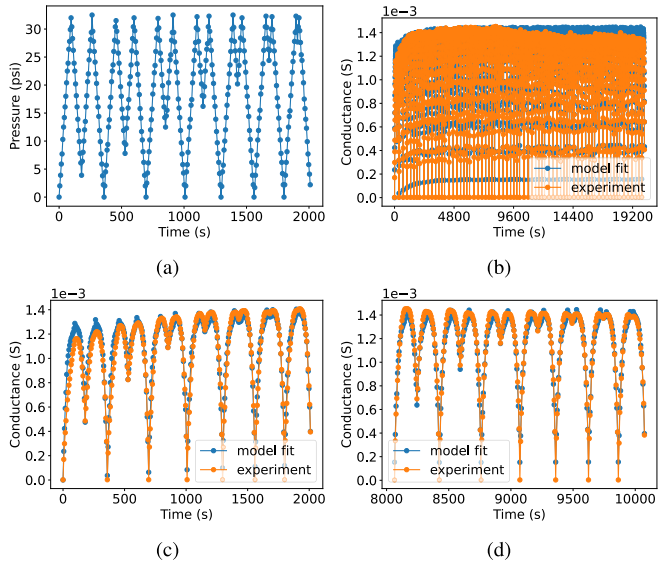

Fig. 6. Experimental results of the ascendant hysteresis cycles. (a) Pressure pattern applied in one repetition. (b) General view of ten repetitions. (c) First repetition. (d) Fifth repetition.

IV. Results and Discussion

A. Model Optimization

The results of the experiments described in Section III-A for model optimization on the small-sized array are presented in Figs. 5 and 6; the former presents the pressure pattern with decreasing maximum values, while the latter presents increasing minimum values. The pressure cycles were repeated ten times consecutively each one. In Fig. 5, the conductance shows an increasing trend as a function of the repetition, while in Fig. 6 the increasing trend takes place up to the intermediate repetitions but then conductance decreases globally in the last ones. Thus, it is clear that the model has to include some dependence on time, which is the creep modeling explained in Section II. The model parameters are shown in Table I. However, the model considered cannot explain the decrease in conductance observed in the last cycles of Fig. 6(b). This behavior is rather another confirmation of the poor repeatability widely highlighted in the literature for piezoresistive sensors [31], [46]. For Velostat-based tactile sensors, previous studies such as [29] and [11] have presented large differences in sensor output for the same load. Dzedzickis et al. [31] indicate that the structure of piezoresistive materials is non-homogeneous, and that this feature has an impact on the repeatability of sensor response. Additionally, they indicate that higher loads can damage Velostat and lead to a loss of conductivity.

TABLE I
Model Parameters

Parameter	Value	Unit
a_1	$1.01 \cdot 10^{-4}$	S/psi
a_2	$-5.32 \cdot 10^{-6}$	S/psi^2
a_3	$7.37 \cdot 10^{-8}$	S/psi^3
ρ	$1.64 \cdot 10^{-4}$	S/psi
τ	0.269	psi^{-1}
l_1	$8.25 \cdot 10^{-4}$	s^{-1}
l_2	$5.26 \cdot 10^{-6}$	s^{-1}
w_1	$8.42 \cdot 10^{-6}$	S/psi
w_2	$1.90 \cdot 10^{-6}$	S/psi
SSE_N	$2.74 \cdot 10^{-9}$	S^2

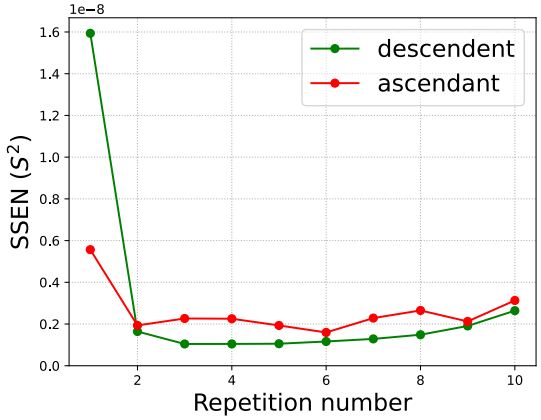

Fig. 7. Results of SSE_N calculated for each repetition of the hysteresis cycles: ascendant cycles (red) and descendent cycles (green).

The figures also show two repetitions in detail to observe the model fit more clearly. The model fit is rather irregular with respect to the cycle repetition. The first repetition is the worse while the fit improves for the next repetitions [compare Fig. 5(c) with Fig. 5(d) or Fig. 6(c) with Fig. 6(d)]. If SSE_N is calculated separately for each repetition, the irregular fit can be quantified, Fig. 7. The main outcome is the anomaly of SSE_N in the first repetition, while the rest is far more homogeneous with some possible trend to get worse for the last repetitions. The difference of the first repetition can be related to the fact that a preload step helps to reduce creep and make the output more repeatable [47], [48]. The well-known manufacturer Tekscan call this conditioning: The sensors should be loaded with a value higher than the maximum load for a few cycles [49], [50], [51]. In our experiment, the first repetition acts as

TABLE II
MODELS USED FOR OBTAINING COP TRAJECTORY

Short name	Comment
FP	Force Platform. The reference instrument in balance tests
PROP	Proportional model. Pressure and conductance are assumed to be proportional in PSM
CHC	Creep and Hysteresis Compensation model for PSM. The joint model explained in section II-C. No scaling is performed.
SCHC	Scaled Creep and Hysteresis Compensation model for PSM. As CHC but introducing a scaling factor, section II-E

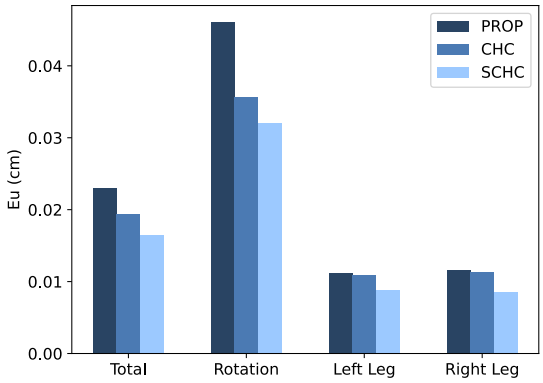

Fig. 8. Averaged results for *Eu* in global and by experiment for three conductance versus pressure models: proportional model (PROP), and creep and hysteresis compensation with or without scaling (SCHC and CHC, respectively).

a kind of preload that reduces the creep of the subsequent repetitions.

B. Center of Pressure

The figure of merit for the CoP experiments on the PSM (Section III-B) is presented for several model variants. The list of abbreviations is included in Table II for the sake of clarity. FP is also included for completeness. Concerning the PSM, results from a naive approach that assumes that conductance is proportional to pressure will be shown (PROP for short). This assumption is sometimes used in the literature and gives a reasonable similarity between the shape of the CoP trajectories derived from PSM and FP. Besides, *Eu* will be shown for two models that compensate hysteresis and creep without and with scaling factor (described in Section II-E), creep and hysteresis compensation (CHC), and scaled CHC (SCHC), respectively.

Fig. 8 shows the figure of merit for the CoP experiments considering the PSM model variants described in Table II. It is apparent from the figure that the models including compensation, CHC and SCHC, improve the naive PROP approach. Scaling is also a relevant aspect to further improve the results, especially in the single-legged experiments (CHC versus SCHC). For these kind of experiments, there is almost no improvement if the scaling is not carried out.

The improvement is also visually apparent when drawing the temporal series of the CoP coordinates. Fig. 9 shows one example of the medial lateral (ML) and anterior posterior (AP) CoP coordinates given by the FP or the PSM considering

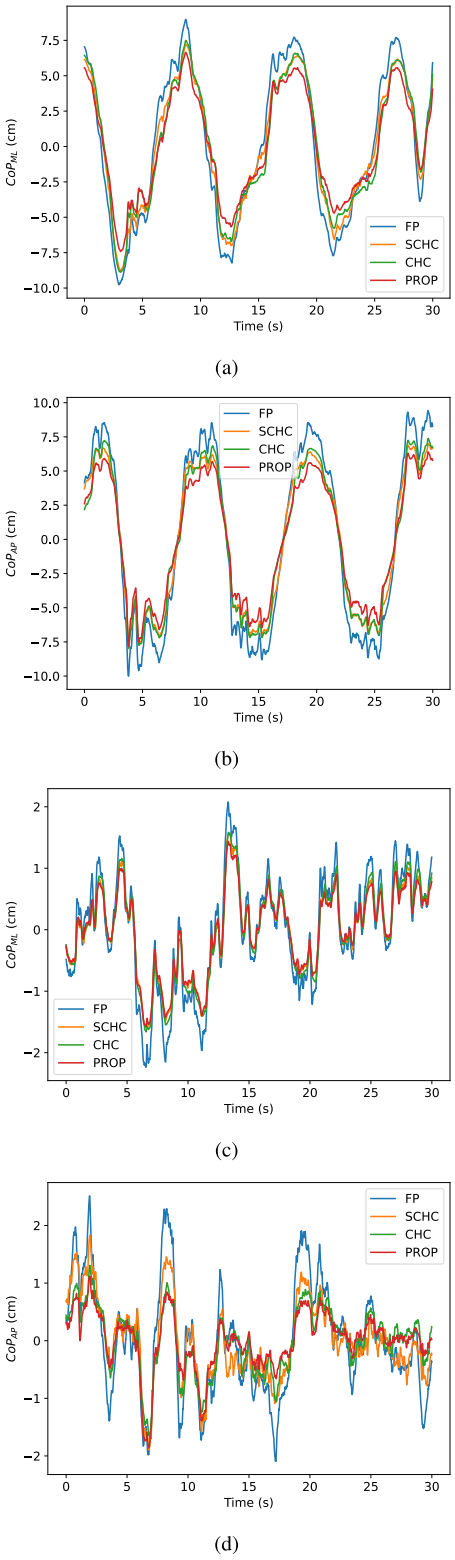

Fig. 9. Examples of temporal series of CoP coordinates. Blue: CoP given by the FP; orange: CoP derived from PSM using the SCHC model; green: CoP derived from PSM using the CHC model; red: CoP obtained from PSM using the PROP model. (a) and (b) Rotation experiment (CoP ML and AP axes, respectively). (c) and (d) Left leg experiment (CoP ML and AP axes, respectively).

a naive PROP approach, the CHC or the SCHC proposed models. Although the correlation between signals is always high, the height of peaks and valleys is clearly different when

comparing the FP and the PSM outputs. Nevertheless, the results of the joint MPI and creep models allow the peaks and valleys of the predicted PSM output to better approximate the results of the FP. SCHC and CHC signals are often very close, but in the AP direction of the single-legged experiment, Fig. 9(d), the scaling, SCHC, seems to make a difference in order to reproduce some peaks. It has been noticed that this is a general trend and not only true for the examples shown in Fig. 9(c) and (d): There is more room for improvement in the AP direction than in the ML direction for single-legged experiments and the scaling is especially relevant in those cases. One of the volunteers repeated the experiments with the same instrument set-up but with his body rotated 90° and the AP direction was again the worse, while it corresponded to a different axis of the instruments. Thus, there seems to be no intrinsic differences between the axes in the PSM.

We have also checked that Eu improved in all the 12 experiments (four people and three trials per person). The average relative improvement of the SCHC model with respect to the PROP model is 26%, ranging from 13% to 37%. Moreover, scaling always improves Eu: when comparing SCHC and CHC, Eu is better again in all the 12 experiments (average relative improvement of 15%, ranging from 2.5% to 34%). Thus, despite the fact that the model has been optimized for a different sample of the sensor array and the approximation inherent to the proposed scaling, it seems that the model has captured a key aspect of the material/electrode behavior.

V. Conclusion and Future Work

In this article, a hysteresis and creep model of a Velostat-based PSM has been found. The model allows measuring the CoP displacements in human stability test with an increasing accuracy. To deduce the model, a small-sized sensor array was subjected to an experiment in a controlled environment with a pneumatic device. A scaling factor was proposed to apply it to the larger mat meaningfully. The experiments show that the model output fits correctly the experimental data. Moreover, when processing the CoP, a clear improvement is observed if the SCHC model is applied (26% in average). In this way, the CoP trajectory measured by a low-cost PSM is more similar to that measured by an FP.

However, the model can be further improved because the fit is far from perfect. Thus, a future work should apply a different characterization that better captures the temporal trend of the sensor output or even to define a model specific to Velostat.

Another aspect to be considered is the large variability of cells between the same array. It is likely that a smaller spatial resolution could alleviate this problem, because the measurement would come from a large number of cells. Nonetheless, a practical procedure to calibrate an equilibrate each cell should be devised for large mats. Another solution would be to be able to build large mats by joining small-sized arrays, each of which could fit the size of pneumatic devices for their characterization.

Acknowledgment

Javier Martínez-Cesteros is with the EduQTech, E.U. Politécnica, University of Zaragoza, 44003 Teruel, Spain (e-mail: javimzcs@unizar.es).

Carlos Medrano-Sánchez and Inmaculada Plaza-García are with the EduQTech, E.U. Politécnica, University of Zaragoza, 44003 Teruel, Spain, and also with the IIS Aragón, University of Zaragoza, 50009 Zaragoza, Spain (e-mail: ctmedra@unizar.es; inmap@unizar.es).

Julián Castellanos-Ramos is with the Departamento de Electrónica, Universidad de Málaga, 29071 Málaga, Spain, and also with the Instituto de Investigación Biomédica de Málaga, 29590 Málaga, Spain (e-mail: jcramos@uma.es).

José A. Sánchez-Durán is with the Departamento de Electrónica, Universidad de Málaga, 29071 Malaga, Spain, and also with the Instituto Universitario de Investigación en Ingeniería Mecatrónica y Sistemas Ciberfísicos (I3MSC), 29071 Malaga, Spain (e-mail: jsd@uma.es).

References

[1] J. Saenz-Cogollo, M. Pau, B. Fraboni, and A. Bonfiglio, "Pressure mapping mat for tele-home care applications," *Sensors*, vol. 16, no. 3, p. 365, Mar. 2016. [Online]. Available: http://www.mdpi.com/1424-8220/16/3/365

[2] S. Nizami, A. Bekele, M. Hozayen, K. J. Greenwood, J. Harrold, and J. R. Green, "Measuring uncertainty during respiratory rate estimation using pressure-sensitive mats," *IEEE Trans. Instrum. Meas.*, vol. 67, no. 7, pp. 1535–1542, Jul. 2018.

[3] Z. Li, Y.-Y. Liang, L. Wang, J. Sheng, and S.-J. Ma, "Reliability and validity of center of pressure measures for balance assessment in older adults," *J. Phys. Therapy Sci.*, vol. 28, no. 4, pp. 1364–1367, 2016.

[4] F. Quijoux et al., "Center of pressure displacement characteristics differentiate fall risk in older people: A systematic review with meta-analysis," *Ageing Res. Rev.*, vol. 62, Sep. 2020, Art. no. 101117. [Online]. Available: https://www.sciencedirect.com/science/article/pii/S156816372030252X

[5] A. Bellicha, A. Trujillo-León, F. Vérité, and W. Bachta, "Analysis of light grip influence on standing posture," *Sensors*, vol. 21, no. 24, p. 8191, Dec. 2021. [Online]. Available: https://www.mdpi.com/1424-8220/21/24/8191

[6] K. Nomura, K. Fukada, T. Azuma, T. Hamasaki, S. Sakoda, and T. Nomura, "A quantitative characterization of postural sway during human quiet standing using a thin pressure distribution measurement system," *Gait Posture*, vol. 29, no. 4, pp. 654–657, Jun. 2009. [Online]. Available: http://www.sciencedirect.com/science/article/pii/S0966636209000526

[7] J. Goetschius, M. A. Feger, J. Hertel, and J. M. Hart, "Validating center-of-pressure balance measurements using the MatScan® pressure mat," *J. Sport Rehabil.*, vol. 27, no. 1, pp. 1–5, Jan. 2018.

[8] C. Bickley, J. Linton, E. Sullivan, K. Mitchell, G. Slota, and D. Barnes, "Comparison of simultaneous static standing balance data on a pressure mat and force plate in typical children and in children with cerebral palsy," *Gait Posture*, vol. 67, pp. 91–98, Jan. 2019. [Online]. Available: http://www.sciencedirect.com/science/article/pii/S0966636218314012

[9] R. A. Ard et al., "Validation of the Tekscan strideway plantar pressure mat compared to a force platform: 1348 board #110 May 30 10:30 AM–12:00 PM," *Med. Sci. Sports Exerc.*, vol. 51, no. 6S, pp. 357–358, 2019.

[10] J. Martinez-Cesteros, C. Medrano-Sanchez, I. Plaza-Garcia, R. Igual-Catalan, and S. Albiol-Pérez, "A Velostat-based pressure-sensitive mat for center-of-pressure measurements: A preliminary study," *Int. J. Environ. Res. Public Health*, vol. 18, no. 11, p. 5958, Jun. 2021. [Online]. Available: https://www.mdpi.com/1660-4601/18/11/5958

[11] D. Giovanelli and E. Farella, "Force sensing resistor and evaluation of technology for wearable body pressure sensing," *J. Sensors*, vol. 2016, pp. 1–13, Jan. 2016.

[12] J. Tolvanen, J. Hannu, and H. Jantunen, "Hybrid foam pressure sensor utilizing piezoresistive and capacitive sensing mechanisms," *IEEE Sensors J.*, vol. 17, no. 15, pp. 4735–4746, Aug. 2017.

[13] S. Nizami, M. Cohen-McFarlane, J. R. Green, and R. Goubran, "Comparing metrological properties of pressure-sensitive mats for continuous patient monitoring," in *Proc. IEEE Sensors Appl. Symp. (SAS)*, Mar. 2017, pp. 1–6.

[14] D. A. Valle-Lopera, A. F. Castraño-Franco, J. Gallego-Londoño, and A. M. Hernández-Valdivieso, "Test and fabrication of piezoresistive sensors for contact pressure measurement," *Revista Facultad Ingeniería Universidad Antioquia*, vol. 10, no. 82, pp. 47–52, Mar. 2017.

[15] J. Sánchez-Durán, J. Hidalgo-López, J. Castellanos-Ramos, Ó. Oballe-Peinado, and F. Vidal-Verdú, "Influence of errors in tactile sensors on some high level parameters used for manipulation with robotic hands," *Sensors*, vol. 15, no. 8, pp. 20409–20435, Aug. 2015. [Online]. Available: https://www.mdpi.com/1424-8220/15/8/20409

[16] J.-F. Wu, "Scanning approaches of 2-D resistive sensor arrays: A review," *IEEE Sensors J.*, vol. 17, no. 4, pp. 914–925, Feb. 2017.

[17] P. A. Misiewicz, K. Blackburn, T. E. Richards, J. L. Brighton, and R. J. Godwin, "The evaluation and calibration of pressure mapping system for the measurement of the pressure distribution of agricultural tyres," *Biosyst. Eng.*, vol. 130, pp. 81–91, Feb. 2015. [Online]. Available: http://www.sciencedirect.com/science/article/pii/S1537511014002219

[18] D. V. Sabarianand, P. Karthikeyan, and T. Muthuramalingam, "A review on control strategies for compensation of hysteresis and creep on piezoelectric actuators based micro systems," *Mech. Syst. Signal Process.*, vol. 140, Jun. 2020, Art. no. 106634. [Online]. Available: https://www.sciencedirect.com/science/article/pii/S0888327020300200

[19] G.-Y. Gu, L.-M. Zhu, C.-Y. Su, H. Ding, and S. Fatikow, "Modeling and control of piezo-actuated nanopositioning stages: A survey," *IEEE Trans. Autom. Sci. Eng.*, vol. 13, no. 1, pp. 313–332, Jan. 2016.

[20] K. K. Leang, Q. Zou, and S. Devasia, "Feedforward control of piezoactuators in atomic force microscope systems," *IEEE Control Syst.*, vol. 29, no. 1, pp. 70–82, Feb. 2009.

[21] J. A. Sánchez-Durán, Ó. Oballe-Peinado, J. Castellanos-Ramos, and F. Vidal-Verdú, "Hysteresis correction of tactile sensor response with a generalized Prandtl–Ishlinskii model," *Microsyst. Technol.*, vol. 18, nos. 7–8, pp. 1127–1138, Aug. 2012.

[22] Y. Chuan and L. Chen, "The compensation for hysteresis of silicon piezoresistive pressure sensor," *IEEE Sensors J.*, vol. 11, no. 9, pp. 2016–2021, Sep. 2011.

[23] J. Sánchez-Durán, F. Vidal-Verdú, Ó. Oballe-Peinado, J. Castellanos-Ramos, and J. Hidalgo-López, "A new model based on adaptation of the external loop to compensate the hysteresis of tactile sensors," *Sensors*, vol. 15, no. 10, pp. 26170–26197, Oct. 2015. [Online]. Available: https://www.mdpi.com/1424-8220/15/10/26170

[24] H. Lee, H. Cho, S. J. Kim, Y. Kim, and J. Kim, "Dispenser printing of piezo-resistive nanocomposite on woven elastic fabric and hysteresis compensation for skin-mountable stretch sensing," *Smart Mater. Struct.*, vol. 27, no. 2, Jan. 2018, Art. no. 025017, doi: 10.1088/1361-665x/aaa5e3.

[25] A. Arndt, "Correction for sensor creep in the evaluation of long-term plantar pressure data," *J. Biomech.*, vol. 36, no. 12, pp. 1813–1817, Dec. 2003. [Online]. Available: https://www.sciencedirect.com/science/article/pii/S002192900300229X

[26] S. R. Chacko and S. M. Sivakumar, "A procedure for correction of creep in foam rubber optical pressure measurement techniques," *Experim. Mech.*, vol. 39, no. 2, pp. 125–131, Jun. 1999.

[27] S. Urban, M. Ludersdorfer, and P. van der Smagt, "Sensor calibration and hysteresis compensation with heteroscedastic Gaussian processes," *IEEE Sensors J.*, vol. 15, no. 11, pp. 6498–6506, Nov. 2015.

[28] S. S. Suprapto, A. W. Setiawan, H. Zakaria, W. Adiprawita, and B. Supartono, "Low-cost pressure sensor matrix using velostat," in *Proc. 5th Int. Conf. Instrum., Commun., Inf. Technol., Biomed. Eng. (ICICI-BME)*, Nov. 2017, pp. 137–140.

[29] R. Barba, Á. P. de Madrid, and J. G. Boticario, "Development of an inexpensive sensor network for recognition of sitting posture," *Int. J. Distrib. Sensor Netw.*, vol. 11, no. 8, Aug. 2015, Art. no. 969237, doi: 10.1155/2015/969237.

[30] D. Z. M. Ramirez, M. del Pilar Garcia Souto, B. M. Oldfrey, P. Smitham, M. Miodownik, and C. Holloway, "Characterization of bespoke force sensors for tailored applications," *IEEE Sensors J.*, vol. 17, no. 6, pp. 1727–1734, Mar. 2017.

[31] A. Dzedzickis et al., "Polyethylene-carbon composite (Velostat®) based tactile sensor," *Polymers*, vol. 12, no. 12, p. 2905, Dec. 2020. [Online]. Available: https://www.mdpi.com/2073-4360/12/12/2905

[32] G.-Y. Gu, L.-M. Zhu, and C.-Y. Su, "Modeling and compensation of asymmetric hysteresis nonlinearity for piezoceramic actuators with a modified Prandtl–Ishlinskii model," *IEEE Trans. Ind. Electron.*, vol. 61, no. 3, pp. 1583–1595, Mar. 2014.

[33] P. Krejci and K. Kuhnen, "Inverse control of systems with hysteresis and creep," *IEE Proc.-Control Theory Appl.*, vol. 148, no. 3, pp. 185–192, May 2001. [Online]. Available: https://digital-library.theiet.org/content/journals/10.1049/ip-cta_20010375

[34] B. Mokaberi and A. A. G. Requicha, "Compensation of scanner creep and hysteresis for AFM nanomanipulation," *IEEE Trans. Autom. Sci. Eng.*, vol. 5, no. 2, pp. 197–206, Apr. 2008.

[35] Z. Sun, B. Song, N. Xi, R. Yang, L. Hao, and L. Chen, "Scan range adaptive hysteresis/creep hybrid compensator for AFM based nanomanipulations," in *Proc. Amer. Control Conf.*, Jun. 2014, pp. 1619–1624.

[36] Z. Chen, L. Hao, D. Xue, X. Xu, and Y. Liu, "Modeling and control with hysteresis and creep of ionic polymer-metal composite (IPMC) actuators," in *Proc. Chin. Control Decis. Conf.*, Jul. 2008, pp. 865–870.

[37] C. Robert and G. Casella, *Monte Carlo Statistical Methods*. Cham, Switzerland: Springer Verlag, 2004.

[38] Y. Tao et al., "A comparative analysis of trajectory similarity measures," *GISci. Remote Sens.*, vol. 58, no. 5, pp. 643–669, Jul. 2021, doi: 10.1080/15481603.2021.1908927.

[39] Tekscan. *PB100E Equilibration Device*. Accessed: Jan. 25, 2023. [Online]. Available: https://www.tekscan.com/products-solutions/equilibrators/pb100e-equilibration-device

[40] *Pneumax Regulador de Presión Proporcional*. Accessed: Jan. 25, 2023. [Online]. Available: https://pneumaxspa.com/en/product-news/regolatori-proporzionali-serie-1700-versione-ethercat/

[41] *Official website of PASCO*. Accessed: Dec. 30, 2022. [Online]. Available: https://www.pasco.com/products/sensors/force/ps-2141

[42] W. Li, C. Sun, W. Yuan, W. Gu, Z. Cui, and W. Chen, "Smart mat system with pressure sensor array for unobtrusive sleep monitoring," in *Proc. 39th Annu. Int. Conf. IEEE Eng. Med. Biol. Soc. (EMBC)*, Jul. 2017, pp. 177–180.

[43] W. Xu, M.-C. Huang, N. Amini, L. He, and M. Sarrafzadeh, "ECushion: A textile pressure sensor array design and calibration for sitting posture analysis," *IEEE Sensors J.*, vol. 13, no. 10, pp. 3926–3934, Oct. 2013.

[44] C. Medrano-Sánchez, R. Igual-Catalán, V. H. Rodríguez-Ontiveros, and I. Plaza-García, "Circuit analysis of matrix-like resistor networks for eliminating crosstalk in pressure sensitive mats," *IEEE Sensors J.*, vol. 19, no. 18, pp. 8027–8036, Sep. 2019.

[45] J. Martinez-Cesteros, C. Medrano-Sanchez, I. Plaza-Garcia, and R. Igual-Catalan, "Uncertainty analysis in the inverse of equivalent conductance method for dealing with crosstalk in 2-D resistive sensor arrays," *IEEE Sensors J.*, vol. 22, no. 1, pp. 373–384, Jan. 2022.

[46] Y. Peng, N. Yang, Q. Xu, Y. Dai, and Z. Wang, "Recent advances in flexible tactile sensors for intelligent systems," *Sensors*, vol. 21, no. 16, p. 5392, Aug. 2021. [Online]. Available: https://www.mdpi.com/1424-8220/21/16/5392

[47] Z. Wang, Y. Dong, H. Zhu, and G. Feng, "Creep characteristics of combined bulk acoustic wave quartz resonator force sensors," *Sens. Actuators A, Phys.*, vol. 111, nos. 2–3, pp. 203–209, Mar. 2004. [Online]. Available: https://www.sciencedirect.com/science/article/pii/S0924424703005727

[48] J. Castellanos-Ramos, "Caracterización, modelado y diseño de sensores táctiles piezorresistivos," Ph.D. dissertation, Departamento de Electrónica, Universidad de Málaga, Málaga, Spain, 2016. [Online]. Available: https://riuma.uma.es/xmlui/handle/10630/11333

[49] Tekscan. *FAQ: Why Do You Need to Condition a Flexiforce Sensor?* Accessed: Jul. 26, 2023. [Online]. Available: https://www.tekscan.com/support/faqs/why-do-you-need-condition-flexiforce-sensor

[50] Tekscan. *Calibration Quick Start Guide for Flexiforce Sensors*. Accessed: Jul. 26, 2023. [Online]. Available: https://www.tekscan.com/sites/default/files/FLX-QS-Calibration-RevG.pdf

[51] J. M. Brimacombe, D. R. Wilson, A. J. Hodgson, K. C. T. Ho, and C. Anglin, "Effect of calibration method on Tekscan sensor accuracy," *J. Biomech. Eng.*, vol. 131, no. 3, Mar. 2009, Art. no. 034503, doi: 10.1115/1.3005165.